nature photonics

LETTERS

PUBLISHED ONLINE: 7 AUGUST 2017 | DOI: 10.1038/NPHOTON.2017.129

Unidirectional photonic wire laser

Ali Khalatpour[1], John L. Reno[2], Nazir P. Kherani[3] and Qing Hu[1]*

Photonic wire lasers are a new genre of lasers that have a transverse dimension much smaller than the wavelength. Unidirectional emission is highly desirable as most of the laser power will be in the desired direction. Owing to their small lateral dimension relative to the wavelength, however, the mode mostly propagates outside the solid core. Consequently, conventional approaches to attach a highly reflective element to the rear facet, whether a thin film or a distributed Bragg reflector, are not applicable. Here we propose a simple and effective technique to achieve unidirectionality. Terahertz quantum-cascade lasers with distributed feedback (DFB) were chosen as the platform of the photonic wire lasers. Unidirectionality is achieved with a power ratio of the forward/backward of about eight, and the power of the forward-emitting laser is increased by a factor of 1.8 compared with a reference bidirectional DFB laser. Furthermore, we achieved a wall plug power efficiency of ~1%.

Unidirectional emission from a ridge laser is highly desirable as such emission patterns will yield a nearly factor-of-two increase in the output power in the desired direction. In conventional Fabry–Perot laser devices, the unidirectional scheme can be easily implemented by the use of a high-reflectivity (HR) coating or distributed Bragg reflector attached to the rear facet. For a new genre of lasers termed photonic wire lasers[1–3], which are of interests in applications such as ultrafast optical modulation[4] and frequency tuning[5–7], their cross-section is much smaller than the lasing wavelength[8]. As such, a large fraction of the lasing mode propagates outside the solid core. From the equivalence of displacement current and conduction current in the generation of electromagnetic waves, the electric field outside and along the solid core forms a distributed emitter. If the emission from this distributed emitter dominates that from the facet, then a HR coating of the rear facet will have a negligible effect on blocking the backward radiation, which results in a bidirectional emission pattern even with a HR coating. Here we demonstrate a novel scheme to achieve unidirectional emission from linear DFB lasers. By strategically placing monolithic reflectors relative to the DFB grating, we can enhance substantially the wave in the forward direction and suppress the wave in the backward direction.

It is well known that the radiation pattern of a linear DFB laser is the product of the array factor (AF) and the element factor (EF). By nature, the periodicity of the DFB structure makes the AF symmetric in both forward and backward directions. Thus, the only way to achieve an asymmetric unidirectional emission is to design and implement a highly asymmetric EF. Terahertz quantum cascade lasers[9] in metal–metal waveguides[10] with a cross-section of about 10 μm, which is much smaller than the lasing wavelength of ~80 μm, are chosen here as the photonic wire laser platform for their easier fabrication because of the long wavelengths. Furthermore, third-order DFB structures (instead of first-order and even-order DFBs, which are surface emitting) were chosen because of their tight (bidirectional) beam patterns[11–13]. In addition, although not essential for the demonstration of unidirectionality, here we also chose the structure of a third-order DFB coupled with an integrated microstrip antenna for a superior performance in the slope efficiency and a high wall-plug efficiency (WPE) of 0.57% in the single-mode operation[14,15]. A periodic antenna-coupled third-order DFB structure, along with the computed symmetric bidirectional radiation pattern, is illustrated in Fig. 1. In a perfectly phase-matched third-order DFB structure, the periodicity is exactly $\lambda_o/2$, where λ_o is the free-space wavelength of the laser. The laser can be modelled as an array of evenly distributed radiators with a π-phase difference between adjacent radiators, which results in a tight bidirectional beam pattern[13].

The key conceptual development in this work is the deliberate design of an asymmetric element structure to 'skew' the bidirectional EF into a unidirectional one. The schematic and the computed overall emission beam patterns are shown in Fig. 2. In this scheme, we explicitly take advantage of a unique feature of photonic wire lasers, that a large portion of the mode propagates outside the solid core. As in the work in which the lasing frequency of a photonic wire laser can be tuned by accessing and manipulating the mode from outside the solid core[6,7], here we place a reflector that can reflect a large fraction of the lasing mode propagating outside the solid core. Unidirectionality can be achieved by placing the reflector at an asymmetric point of the DFB grating. In this scheme, the EF is the field of a single aperture in the presence of all those passive reflectors. However, through simulations, we realized that the

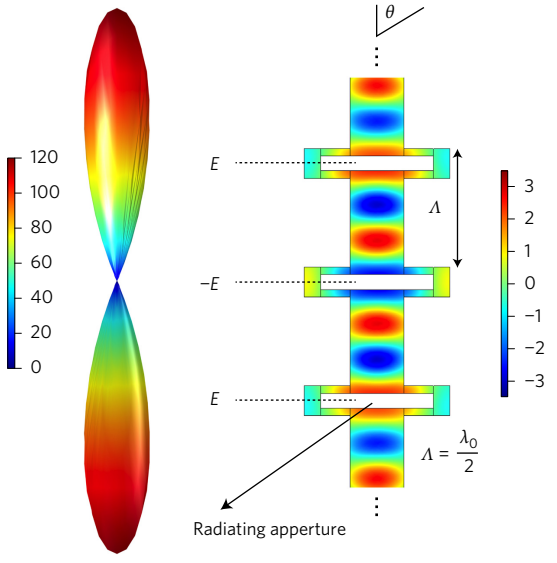

Figure 1 | Distribution of E_z (normal to the page; in arbitrary units) of a third-order DFB laser for the desired mode under a perfect phase-matching condition (right) and the corresponding far-field radiation pattern (left).

[1]Department of Electrical Engineering and Computer Science and Research Laboratory of Electronics, Massachusetts Institute of Technology, Cambridge, Massachusetts 02139, USA. [2]Sandia National Laboratories, Center of Integrated Nanotechnologies, Albuquerque, New Mexico 87185-130, USA. [3]Department of Electrical Engineering and Computer Science, University of Toronto, Ontario M5S 3G4, Canada. *e-mail: qhu@mit.edu

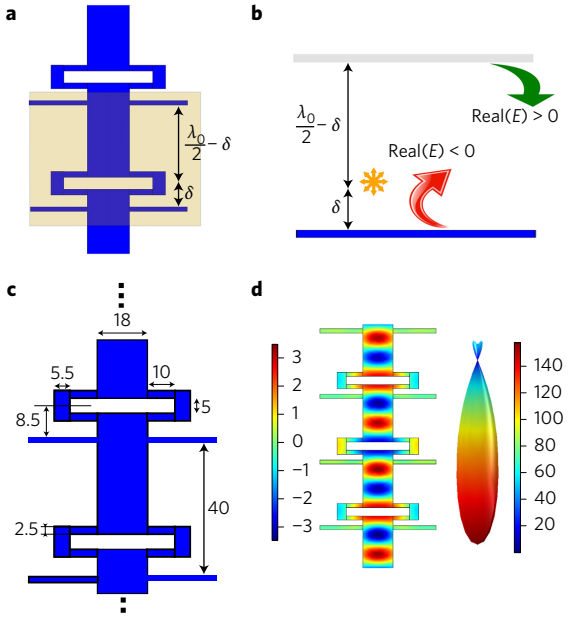

Figure 2 | Simple model for unidirectional third-order DFB. a, The aperture field interacts with the closest reflectors, which act as the new EF. **b**, A simple model that approximates the aperture field as a point source (yellow) interacting with adjacent reflectors. The red arrow indicates a reflected wave that interferes destructively with the radiated field in the backward direction. The green arrow indicates a reflected wave that interferes constructively with the radiated field in the forward direction. **c**, Optimum geometry designed using full wave simulations (the length unit is micrometres). **d**, Simulated distribution for E_z in arbitrary units (left) and the corresponding far-field radiation pattern (right).

aperture field mainly interacts with the closest reflectors. So, for a qualitative understanding based on a simple model, the new EF is the aperture field in the presence of the two closest reflectors to it. This is shown in Fig. 2a. Qualitatively, the aperture of the antenna-coupled DFB structure can be approximated as an omni-directional source that emits symmetrically in both forward and backward directions. The reflector at a distance δ from the aperture, when $\delta < \lambda_o/8$, reflects the aperture field in a way that destructively interferes with the backward radiation and causes a preferential radiation in the forward direction. More quantitatively, the coefficient of the field reflection from vacuum to dielectric is $r = (1 - n)/(1 + n)$ for a transverse-electric plane wave and $r < 0$, which causes a 180° phase shift at the interface. The additional phase shift, from a round-trip travelling with a distance of $\delta < \lambda_o/8$, is <90°, results in a total phase shift of 180° to 270° between the reflected wave and the backward radiation from the aperture to yield a destructive interference. Not obvious, but verified through simulation, there is also a constructive interference in the forward direction because of double reflections from the closest reflectors to the aperture (a double negative-reflection coefficient leads to a positive coefficient). The overall mechanism in our simple model is shown in Fig. 2b. Based on this qualitative understanding, three-dimensional (3D) full-wave finite-element quasi-eigenmode simulations were performed to explore the optimized reflector position and length. The simulation is performed on a 35-element antenna-coupled third-order DFB with the parameters shown in Fig. 2c. The optimum values were found to be $\delta = 8.5\ \mu m < \lambda_o/8$ ($=\Lambda/4$), where Λ is the grating period of a perfectly phase-matched third-order DFB and $\lambda_o \approx 80\ \mu m$. The simulation results are shown in Fig. 2d. A strong asymmetry in the radiation pattern is produced because of the reflectors. In the numerical simulation, we found that the reflector length is not a sensitive design parameter, but it should be longer than the length of the aperture antenna to be

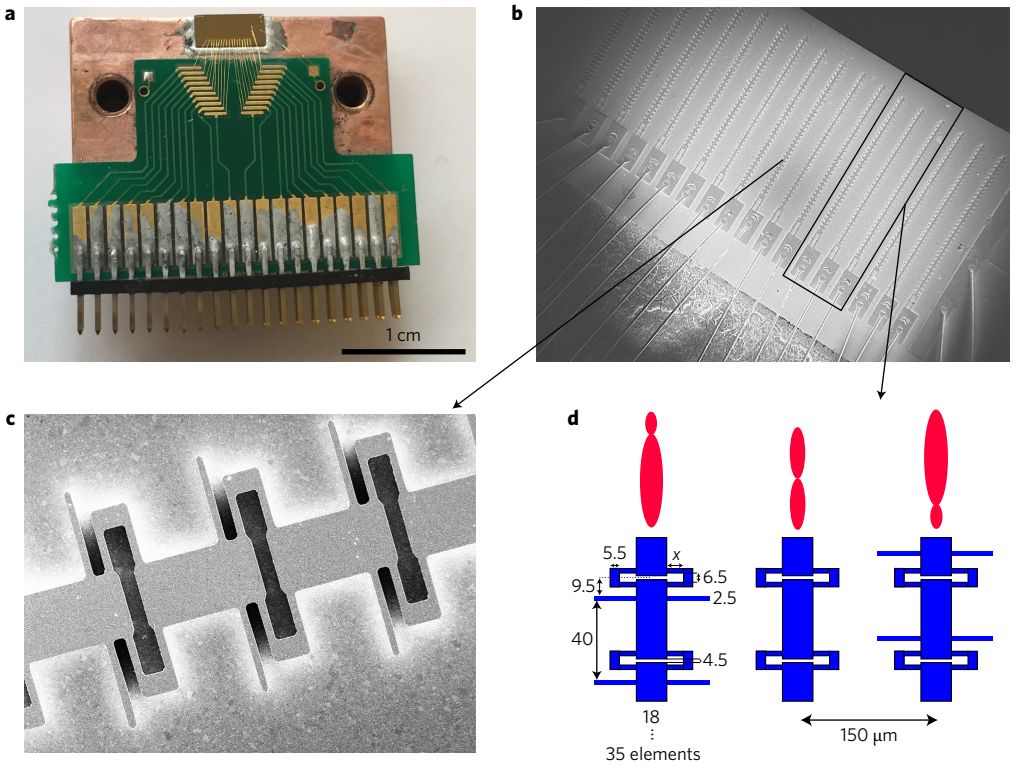

Figure 3 | Fabrication and measurement strategy. a, Array of third-order DFB lasers gold-wire bonded to an electronic chip for nearly simultaneous measurement. **b**, Photos of the fabricated array of DFB triplets. **c**, The SEM of a DFB device shows three periods. **d**, Schematic of a triplet with the corresponding radiation profile (all dimensions are in micrometres).

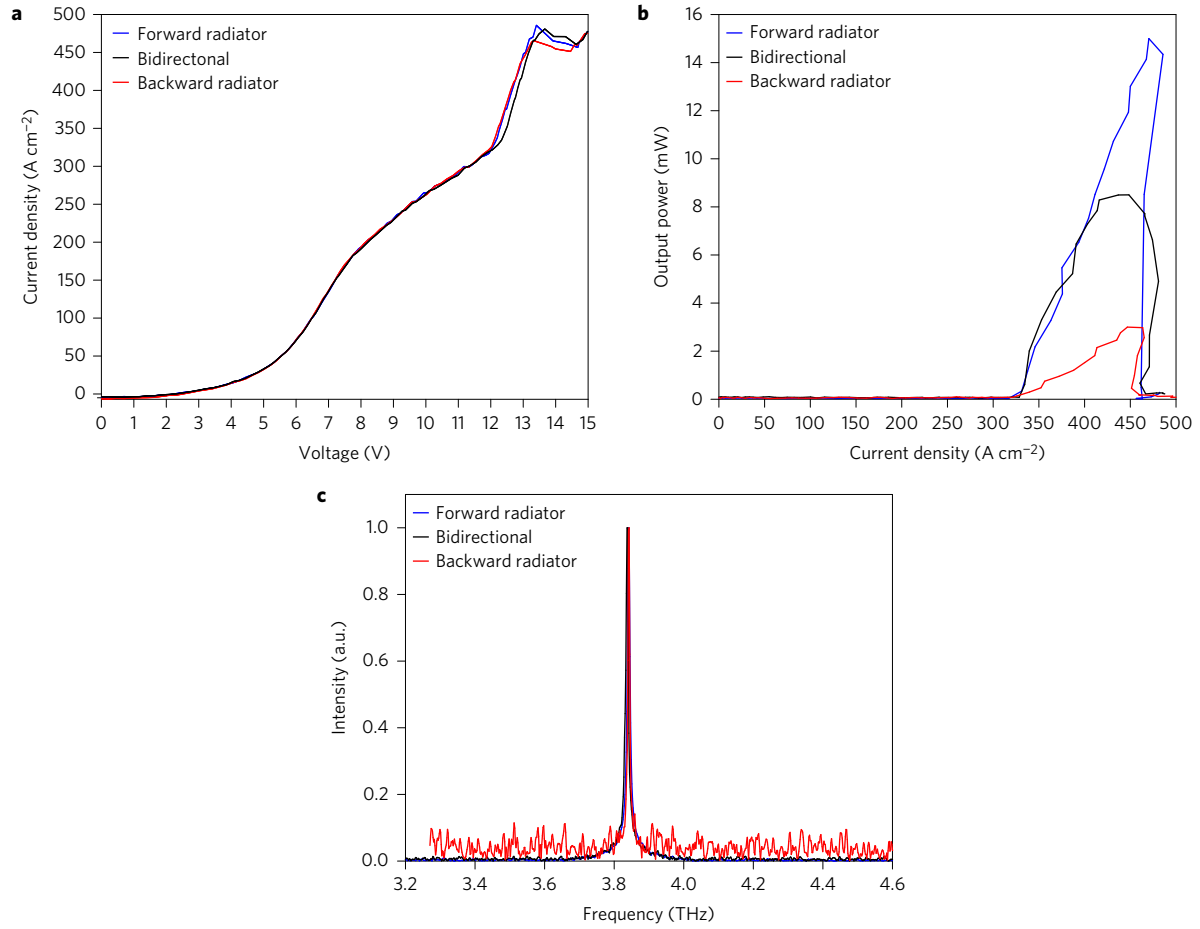

Figure 4 | Measurement results for a unidirectional third-order DFB. a, *V–I* measurement for the triplet with an antenna length of 9.5 μm. **b**, *L–I* measurement. **c**, Frequency spectra of the lasers. The difference in the lasing frequencies is within the instrumental resolution of 3.75 GHz of the FTIR spectrometer. a.u., arbitrary units.

effective as the size of the reflectors affects the constructive interference in the forward direction. A length of 26 μm was chosen based on optimization algorithms in conjunction with a full-wave simulation. The top metal layer on the reflectors has no effect on the unidirectionality, because the electric field is largely normal to the metal strip and so produces negligible surface current.

Several arrays of DFB triplets from this design were fabricated to verify the unidirectionality in the radiation pattern. Each triplet consisted of a DFB with a reflector placed optimally to radiate in the desired direction (forward radiator), a DFB with a reflector that is flipped 180° compared with the one that radiates in the forward direction (backward radiator) and a reference DFB without a reflector, which should have a symmetric bidirectional radiation pattern. The short distance among those three lasers (150 μm) minimizes the variation in device performances caused by fabrication fluctuations. The antenna length (denoted as x in Fig. 3) varies from one triplet to another to achieve the optimum phase-matching condition. The biasing current is provided to the laser array through a large bonding pad on top of a thin (2,500 Å) layer of silicon nitride as an isolation layer. The array is gold-wire bonded to an electronic chip, which enables us to switch the bias electronically among the triplets to provide the same measuring environment. The pulsed current–voltage (I–V) and light–current (L–I) curves for a DFB triplet with an antenna length of 9.5 μm are shown in Fig. 4a,b. The spectra measurement shows a single-mode emission for the triplet at around 3.83 THz. Similar lasing frequency (within 4 GHz) and I–V characteristics confirm that fabrication fluctuation is negligible from one DFB laser to another. The lasing-threshold current densities for the three lasers are also approximately the same, which indicates that all three structures have a similar radiation (mirror) loss, α_m. Clearly, the structure designed for forward emission delivered a much higher power (by a factor of ~8) than that of the backward structure, which shows a clear unidirectional radiation pattern. Furthermore, compared with the reference of a bidirectional DFB, a factor of a 1.8 increase in the output power from the unidirectional laser is obtained, validating the advantage of unidirectionality, which is the original motivation of this work. The measured WPE is 0.87%, which is a good improvement over the previously reported numbers[14,15].

It is well known that power from a laser is proportional to $(\alpha_m/(\alpha_m + \alpha_w))$ in which α_w is the waveguide loss[16]. The lasing threshold of the lasers is proportional to $(\alpha_m + \alpha_w)/\Gamma$ in which Γ is the mode-confinement factor. For the maximum output without a significant increase in the laser threshold, $\alpha_m \approx \alpha_w$. Through 3D full-wave simulations, we noticed that to add a reflector to the DFB decreases the mirror loss slightly (by 2–5 cm^{-1}), because the reflectors increase the feedback, which reduces the radiation loss. Consequently, the parameters for the optimum design of an antenna-coupled third-order DFB without a reflector are not the same as those for the optimum design for a unidirectional DFB. To make a fair comparison of the relative performance, we further increased the mirror loss for unidirectional DFBs (and increasing WPE) by aiming for $\alpha_m = 15$ cm^{-1}, which is the measured waveguide loss α_w in a similar structure[17]. The schematic of the new design along with the scanning electron microscopy (SEM) images of the finished laser cavities are shown in Fig. 5a. The higher mirror loss

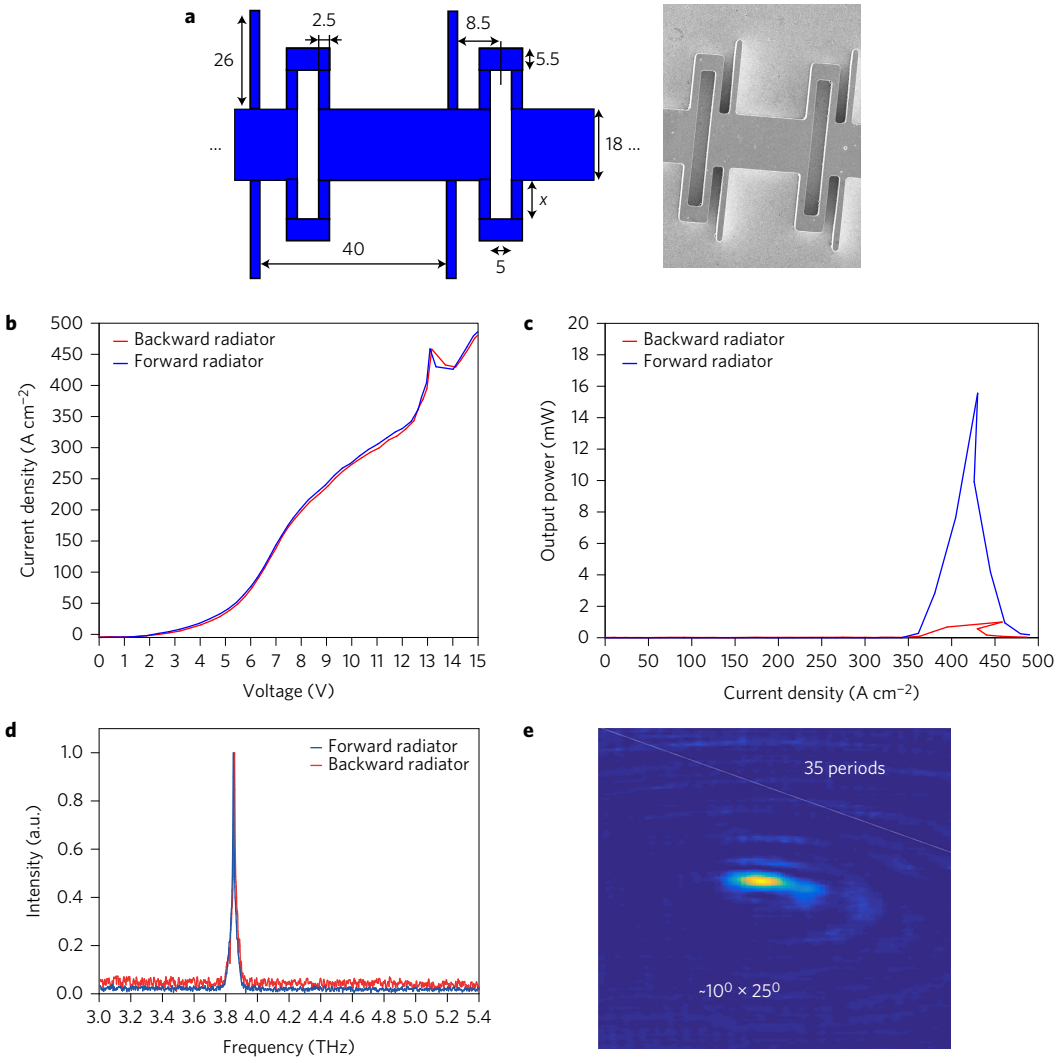

Figure 5 | Measurement results for a unidirectional third-order DFB. a, Schematic of the optimum geometry for the unidirectional DFB with an antenna length of $x = 10$ μm (left) with SEM images (top view) of the finished cavities (right). Notice the gap-shape difference with the extruded gap design in Fig. 3. All the dimensions are in micrometres. **b**, *V*–*I* measurements from the DFBs with $x = 10$ μm. **c**, *L*–*I* measurement. **d**, Frequency spectrum of the lasers. **e**, Single-lobe beam pattern measured with a FLIR camera from the forward radiator.

was achieved (from ~11 cm^{-1} to ~15 cm^{-1}) by increasing the gap size between the cavities and placing the antenna at the gap edge. The measurement results from this design are shown in Fig. 5b–e. The similar *I*–*V* characteristic and close lasing frequency (within 9 GHz) confirm minimal fabrication fluctuations. The maximum power of a forward radiator with an antenna length of 10 μm is 16.1 mW at a bias of $V_d = 13.1$ V and $I_d = 124$ mA. The resultant WPE is about 1%. The single-lobe beam pattern of the laser (Fig. 5e) was confirmed using a FLIR camera[18]. Even though the main purpose of this work is to develop and demonstrate a conceptually novel scheme of unidirectional photonic wire lasers, the absolute performance in terms of WPE is also superior compared with previously reported results from DFB lasers[14,15].

In conclusion, here we present a conceptually novel structure to achieve unidirectional emission from photonic wire lasers and demonstrate clear experimental results to validate the concept. Compared with a conventional bidirectional DFB laser, the unidirectional laser has yielded a greater output power by a factor of 1.8, without any additional fabrication steps or/and external optics. In a structure specifically optimized for the unidirectional lasers, we also achieved a record WPE ≈ 1% for DFB lasers at terahertz frequencies. Clearly, the scheme of unidirectionality can be applied to photonic wire lasers at other wavelengths, but the optimum reflector properties should be determined based on the fabrication process and material availability in the frequency range of interest.

Methods

Methods and any associated references are available in the online version of the paper.

Received 24 February 2017; accepted 3 July 2017;
published online 7 August 2017

References

1. Zhang, J. P. *et al.* Photonic-wire laser. *Phys. Rev. Lett.* **75,** 2678–2681 (1995).
2. Zhang, J. P. *et al.* Directional light output from photonic-wire microcavity semiconductor lasers. *IEEE Photon. Technol. Lett.* **8,** 968–970 (1996).
3. Hill, M. T. & Gather, M. C. Advances in small lasers. *Nat. Photon.* **8,** 908–918 (2014).
4. Altug, H., Englund, D. & Vučković, J. Ultrafast photonic crystal nanocavity laser. *Nat. Phys.* **2,** 484–488 (2006).
5. Ohtani, K., Beck, M. & Faist, J. Electrical laser frequency tuning by three terminal terahertz quantum cascade lasers. *Appl. Phys. Lett.* **104,** 011107 (2014).
6. Qin, Q., Williams, B. S., Kumar, S., Reno, J. L. & Hu, Q. Tuning a terahertz wire laser. *Nat. Photon.* **3,** 732–737 (2009).

7. Han, N. *et al.* Broadband all-electronically tunable MEMS terahertz quantum cascade lasers. *Opt. Lett.* **39,** 3480–3483 (2014).
8. Orlova, E. E. *et al.* Antenna model for wire lasers. *Phys. Rev. Lett.* **96,** 173904 (2006).
9. Williams, B. S. Terahertz quantum-cascade lasers. *Nat. Photon.* **1,** 517–525 (2007).
10. Williams, B. S., Kumar, S., Callebaut, H., Hu, Q. & Reno, J. L. Terahertz quantum cascade laser at $\lambda \approx 100$ μm using metal waveguide for mode confinement. *Appl. Phys. Lett.* **83,** 2124–2126 (2003).
11. Amanti, M. I., Fischer, M., Scalari, G., Beck, M. & Faist, J. Low-divergence single-mode terahertz quantum cascade laser. *Nat. Photon.* **3,** 586–590 (2009).
12. Amanti, M. I., Scalari, G., Castellano, F., Beck, M. & Faist, J. Low divergence terahertz photonic-wire laser. *Opt. Express.* **18,** 6390–6395 (2010).
13. Kao, T.-Y., Hu, Q. & Reno, J. L. Perfectly phase-matched third-order distributed feedback terahertz quantum-cascade lasers. *Opt. Lett.* **37,** 2070–2072 (2012).
14. Kao, T.-Y., Cai, X., Lee, A. W. M., Reno, J. L. & Hu, Q. Antenna coupled photonic wire lasers. *Opt. Express* **23,** 17091–17100 (2015).
15. Xu, G. *et al.* Surface-emitting terahertz quantum cascade lasers with continuous-wave power in the tens of milliwatt range. *Appl. Phys. Lett.* **104,** 091112 (2014).
16. Faist, J. Wallplug efficiency of quantum cascade lasers: critical parameters and fundamental limits. *Appl. Phys. Lett.* **90,** 253512 (2007).
17. Burghoff, D. *et al.* A terahertz pulse emitter monolithically integrated with a quantum cascade laser. *Appl. Phys. Lett.* **98,** 061112 (2011).
18. Lee, A. W. M., Qin, Q., Kumar, S., Williams, B. S. & Hu, Q. Real-time terahertz imaging over a standoff distance (>25 meters). *Appl. Phys. Lett.* **89,** 141125 (2006).

Acknowledgements

This work is supported by the National Aeronautics and Space Administration and the National Science Foundation at the Massachusetts Institute of Technology. This work was performed, in part, at the Center for Integrated Nanotechnologies, an Office of Science User Facility operated for the US Department of Energy Office of Science. Sandia National Laboratories is a multiprogram laboratory managed and operated by Sandia Corporation, a wholly owned subsidiary of Lockheed Martin Corporation, for the US Department of Energy's National Nuclear Security Administration under contract DE-AC04-94AL85000. A.K. acknowledges support from Natural Science and Engineering Research Council of Canada.

Author contributions

A.K. conceived the idea and strategy, designed and fabricated the devices and performed the measurements and analysis, and J.L.R. provided the material growth. A.K. benefited from in-depth discussions regarding the simulation and design strategy with N.P.K. All the work was done under the supervision of Q.H.

Additional information

Supplementary information is available in the online version of the paper. Reprints and permissions information is available online at www.nature.com/reprints. Publisher's note: Springer Nature remains neutral with regard to jurisdictional claims in published maps and institutional affiliations. Correspondence and requests for materials should be addressed to Q.H.

Competing financial interests

The authors declare no competing financial interests.

Methods

Finite element simulations. The simulations were carried out using COMSOL Multiphysics version 5.3. The details are provided in Supplementary Information.

***L–I–V* and spectrum measurement.** For pulsed *L–I–V* measurements, the lasers were operated at 100 kHz with a pulse duration of 1 μs (10% duty cycle) at a temperature of 15 K. The optical power was measured with a QMC Instruments pyroelectric detector with an attached Winston cone for optimum collection, and electronically chopped at 100 Hz. Spectra were measured using a Fourier transform infrared (FTIR) spectrometer (Thermo Nicolet 6700) with a QMC Instruments pyroelectric detector as the external detector.

Power measurement. The relative power measured from the pyroelectric detector was calibrated using a Thomas Keating absolute terahertz power meter at a 30 Hz electronic chopping frequency without any focusing optics between the laser and the power meter except a high-density polyethylene window on the cryostat. The laser under test was operated at 100 kHz with a pulse duration of 1 μs (10% duty cycle) at a temperature of 15 K inside a Cryomech Pulse tube cryorefrigerator (PT 810).

Data availability. The data that support the plots within this paper and other findings of this study are available from the corresponding author on reasonable request.